This article was downloaded by:
On: *21 January 2011*
Access details: *Access Details: Free Access*
Publisher *Taylor & Francis*
Informa Ltd Registered in England and Wales Registered Number: 1072954 Registered office: Mortimer House, 37-41 Mortimer Street, London W1T 3JH, UK

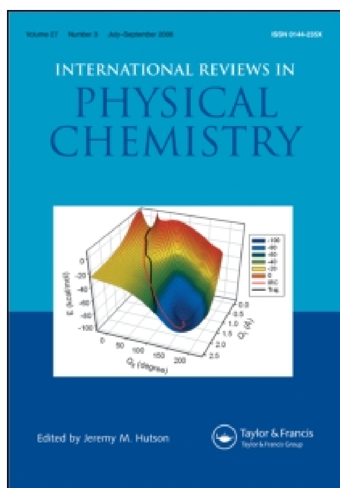

International Reviews in Physical Chemistry
Publication details, including instructions for authors and subscription information:
http://www.informaworld.com/smpp/title~content=t713724383

The picture tells the story: Using surface morphology to probe chemical etching reactions

Melissa A. Hines

Online publication date: 26 November 2010

To cite this Article Hines, Melissa A.(2001) 'The picture tells the story: Using surface morphology to probe chemical etching reactions', International Reviews in Physical Chemistry, 20: 4, 645 — 672
To link to this Article: DOI: 10.1080/01442350110071966
URL: http://dx.doi.org/10.1080/01442350110071966

PLEASE SCROLL DOWN FOR ARTICLE

Full terms and conditions of use: http://www.informaworld.com/terms-and-conditions-of-access.pdf

This article may be used for research, teaching and private study purposes. Any substantial or systematic reproduction, re-distribution, re-selling, loan or sub-licensing, systematic supply or distribution in any form to anyone is expressly forbidden.

The publisher does not give any warranty express or implied or make any representation that the contents will be complete or accurate or up to date. The accuracy of any instructions, formulae and drug doses should be independently verified with primary sources. The publisher shall not be liable for any loss, actions, claims, proceedings, demand or costs or damages whatsoever or howsoever caused arising directly or indirectly in connection with or arising out of the use of this material.

Int. Reviews in Physical Chemistry, 2001, Vol. 20, No. 4, 645–672

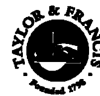

The picture tells the story: using surface morphology to probe chemical etching reactions

MELISSA A. HINES
Department of Chemistry, Cornell University, Ithaca, NY 14853-1301, USA

Highly anisotropic etchants, which only attack specific crystallographic planes of a material, are prized by industry, but the inherent defect selectivity of these etchants has stymied investigations into their chemical mechanism. Because of their chemical specificity, these etchants produce characteristic nanoscale morphological features, such as triangular etch pits and jagged atomic steps, which reflect the site-specific chemical reactions that control the etching. Using a combination of scanning tunnelling microscopy and kinetic Monte Carlo simulations, these site-specific rates can be directly quantified. By correlating these measurements with the structure of the etched sites, information on the reaction mechanism can be obtained. These techniques are illustrated with examples drawn from aqueous silicon etching reactions. For example, the production of atomically flat Si(111) surfaces by NH_4F etching can be explained by the existence of a pentacoordinate transition state to OH^- attack. Sites held in a rigid tetrahedral geometry, such as the Si(111) terrace site, are relatively resistant to attack, while defect sites, such as steps and kinks, are rapidly etched.

Downloaded At: 16:40 21 January 2011

Contents

PAGE

1. Introduction 646

2. The morphology of individual features 647
- 2.1. Vicinal steps 648
- 2.2. Etch pits and islands 650
- 2.3. More complicated features: etch hillocks 652
- 2.4. Setting the scale with interacting etch features 658

3. Extreme anisotropy: the etching of silicon by NH_4F 660
- 3.1. Site-specific rates and chemical mechanism 661
- 3.2. Impurities and other sources of frustration 663

4. Unravelling complexity with kinetic competition: the unusual effects of isopropanol on etching 664
- 4.1. Concentration effects and kinetic competition 666
- 4.2. The mechanism of isopropanol 668

5. Conclusions and outlook 670

Acknowledgements 670

References 670

International Reviews in Physical Chemistry ISSN 0144–235X print/ISSN 1366–591X online © 2001 Taylor & Francis Ltd
http://www.tandf.co.uk/journals
DOI: 10.1080/01442350110071966

1. Introduction

Anisotropic etchants (etchants that selectively reveal specific crystallographic faces) have long fascinated scientists. Decades before X-ray diffraction was even imagined, mineralogists used anisotropic etchants to reveal the inherent symmetry of crystals (Schreibers 1820, Baumhauer 1894). Later, with the birth of the semiconductor industry in the 1950s, it became apparent that very low densities of crystallographic defects, such as dislocations and stacking faults, were degrading the performance of semiconductor devices. Because these defects have atomic dimensions and occur in extremely low densities, atomic-resolution probes would have been impractical even if they had been available. Instead, materials scientists developed solutions that would selectively (i.e. anisotropically) etch defects, leaving behind pits and hillocks visible to the eye (Amelinckx 1964, Sangwal 1987). These etchants were then used to refine crystal growth technology (Dash 1958).

Today, anisotropic etchants are used in many industrial processes. Although aqueous etchants are no longer used for lithographic pattern development in the microelectronics industry, they are the heart of silicon cleaning technology. Since it is generally accepted that over 50% of yield losses in integrated-circuit fabrication are due to microcontamination (Burkman *et al.* 1993), aqueous etching still plays a vital role in the microelectronics industry. Most aqueous bases etch close-packed Si(111) surfaces orders of magnitude more slowly than other surfaces; so these anisotropic etchants can also be used to selectively machine well-aligned Si(111) surfaces. Because of this, anisotropic etching is widely used in the fabrication of silicon micromachines (Elwenspoek and Jansen 1998).

Downloaded At: 16:40 21 January 2011

Not all etchants are anisotropic. Some are in fact quite isotropic. Unfortunately, etchant anisotropy can only be determined by direct measurement; no chemical theory of anisotropy exists. Anisotropy can be most easily visualized in terms of dissolution form experiments in which a single-crystal sphere is etched until its form reaches steady state. For example, Batterman (1957) showed that a germanium sphere will be reduced to a dodecahedron when etched in an aqueous solution of H_2O_2/HF. This shape reflects the slow etching of {111} and {100} planes, and the fast etching of {110} planes. Similarly, Faust (1960) showed that a silicon sphere could be reduced to a cube consisting of {100} planes using the appropriate concentration of NaOH. In contrast, the so-called CP4 etchant, which is composed of HNO_3/HF/Br_2/CH_3COOH, has a spherical limiting shape; it is essentially isotropic.

Chemically, what distinguishes an anisotropic etchant from an isotropic etchant? Clearly, an anisotropic etchant must have a high degree of chemical specificity. This specificity is not to a crystalline face *per se*, however, because etchants do not remove crystal planes intact. Instead, the etchant must be highly *site selective*. For example, Higashi *et al.* (1990) showed that NH_4F(aq) etching of atomically rough Si(111) surfaces produces nearly perfect Si(111) planes. This implies that the etchant selectively attacks defects on the Si(111) surface (e.g. steps, kinks) while leaving the perfect surface (the close-packed plane) essentially untouched. Looking at the problem in this light, it is clear that an anisotropic etchant must be highly *defect selective*.

Although defect selectivity is the hallmark of anisotropic etching, this selectivity has severely hindered our chemical understanding of the process. Since the density of surface defect sites is typically well below the sensitivity limit of surface spectroscopies, these sites are 'invisible' to most techniques. As such, anisotropic etching

reactions have often been mistakenly explained in terms of the reactivity of the majority species, the terrace site.

There is one surface science technique that is uniquely sensitive to defects, namely scanning tunnelling microscopy (STM). Although STM has little inherent chemical sensitivity, anisotropic etching literally writes a record of the reactivity of the etchant into the etched surface morphology. In the same way that fast- and slow-etching planes of a crystal are recorded in the polyhedral shapes of dissolution form experiments, the atomic-scale surface morphology also develops characteristic etch features, such as triangular etch pits and jagged step edges, which are direct records of defect site reactivity. Like the macroscopic forms, the atomic-scale morphology reaches a steady state after prolonged etching which is dependent only on the etching chemistry; no memory of the initial surface morphology is retained. These characteristic etch morphologies convey a great deal of information to the trained eye. In addition, computer simulations of the etching process can be used to extract quantitative estimates of the site-specific reaction rates. When combined with information about defect site structure, these rates provide clues to the underlying chemical mechanisms.

In the following, I shall illustrate these techniques using examples drawn from our own studies of Si(111) etching in various aqueous solutions.

Downloaded At: 16:40 21 January 2011

2. The morphology of individual features

Chemical etching can have a profound effect on surface morphology as shown by the two images in figure 1. The image in figure 1 (*a*) is a typical morphology of an unetched, highly polished silicon wafer. (More correctly, this image depicts the structure of an annealed Si–SiO_2 interface after the oxide has been stripped with HF(aq).) Although this wafer is miscut by 0.3° from the Si(111) surface and thus has a step–step spacing of about 50 nm, the extreme roughness of the surface obscures the morphology of the vicinal steps. The surface features are also very amorphous, and there is no hint of the underlying threefold symmetry of the lattice.

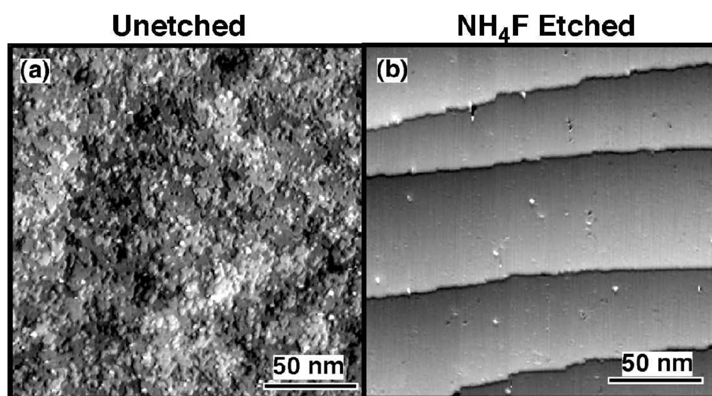

Figure 1. STM images of etched Si(111). (*a*) Thermally oxidized Si(111) etched for 2 min in buffered HF (Transene; 7:1 mix of aqueous HF/NH_4F). The morphology reflects the original Si–SiO_2 interface. (*b*) Si(111) surface miscut by 0.3° in the $\langle 11\bar{2} \rangle$ direction and etched in 40% NH_4F(aq) for 60 min in a N_2 ambient.

After etching in 40% $NH_4F(aq)$, the surface morphology is completely transformed, as illustrated by figure 1 (*b*). This etchant selectively removes all the original roughness and produces a surface that is almost, but not quite, perfect. In particular, the vicinal steps are now the most prominent feature on the surface. Between these steps, there are large regions of perfect Si(111), with no missing or extra silicon atoms. The surface is not truly perfect, however, as there is a low density of monolayer deep etch pits. (The white dots are contaminants, as discussed in section 2.4.) In this image, most of the pits appear to be amorphous owing to the finite resolution of the tip; however, a close examination of the larger pits reveals a pronounced triangular shape. Although not apparent from this image, infrared spectroscopy shows that there are no dangling bonds on this surface. Instead, the surface is terminated by a monolayer of hydrogen. Interestingly, most of the site-specific chemistry that caused this transformation from rough to smooth can be inferred from the etched surface morphology itself. The two most important clues are the very straight vicinal steps and the tiny triangular pits, which we shall discuss in turn. Following this, we shall discuss a somewhat more esoteric feature, namely the etch hillock, and then finish our discourse with a discussion of interacting step features. The examples in this section are all drawn from our investigations of NH_4F etching of the various miscuts of Si(111).

Downloaded At: 16:40 21 January 2011

2.1. *Vicinal steps*

Vicinal steps are perhaps the most revealing probe of etchant chemistry, because these steps are the only controllable source of surface defects. The orientation of the surface miscut controls the structure of the surface steps, while the magnitude of the miscut controls the step density. On Si(111), there are two principle miscuts (i.e. close-packed step directions). Surfaces miscut towards the $\langle 11\bar{2}\rangle$ direction have monohydride-terminated steps, while surfaces miscut towards the $\langle \bar{1}\bar{1}2\rangle$ direction have dihydride-terminated steps. Because of the threefold symmetry of the surface, there are three equivalent steps of each type, rotated by 60° from one another.

Figure 2 illustrates the chemical structure of the various surface sites. Unfortunately, STM cannot provide the level of chemical detail needed to construct this sketch, which is instead based on the extensive studies of Chabal and co-workers on the infrared and Raman spectra of etched surfaces (see for example Trucks *et al.* (1990), Jakob and Chabal (1991) and Hines *et al.* (1993, 1994)). By analysing the characteristic polarization dependence of the various Si—H vibrational modes observed on surfaces with a high step density (about 9° miscut), precise information about the chemical structure of the various silicon hydride species that terminate step edges could be obtained. For example, the complex mode structure of the dihydride-terminated step provided conclusive evidence of severe strain between the dihydride species and a Si—H on the terrace below, whereas the pronounced polarization of the absorption features perpendicular to the step could only be explained by a *vertical* structure (Jakob and Chabal 1991). Although the kink site is present in concentrations too low to be observed by vibrational spectroscopy, the geometry of this site can be inferred from the geometry of the other step sites.

Neglecting the detailed structure of the actual steps for the moment, a close-packed step must have at least two types of reactive sites: the close-packed step site and the kink site. In this simple case, the morphology of the etched steps can be understood in terms of the competition between these two reactive sites. Two kink sites are nucleated when a step site is etched from an otherwise perfect step. Once

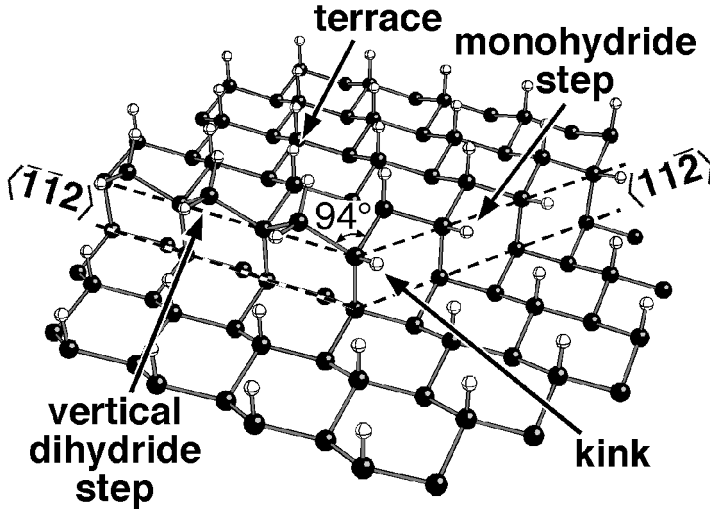

Figure 2. The atomic structure of Si(111) surfaces etched in aqueous solutions. The dark spheres represent silicon atoms, while the light spheres represent hydrogen atoms. The geometry of the step sites was determined by Chabal and co-workers using vibrational spectroscopy. The vertical dihydride site is severely strained by interactions with a hydrogen atom on the terrace below. Because of this, the kink site is also severely distorted.

Downloaded At: 16:40 21 January 2011

formed, subsequent etching of a kink site removes one step atom and generates a new kink at the neighbouring site. When repeated many times, sequential kink etching effectively leads to the 'unzipping' of a single row of atoms from the edge of a vicinal step. This process tends to straighten rough steps. Kink nucleation, on the other hand, corresponds to etching into the step, which increases the roughness of the step. Qualitatively, straight steps are formed when unzipping dominates kink nucleation, whereas rough steps are formed when nucleation dominates.

These simple arguments can be made quantitative using an atomistic kinetic Monte Carlo (KMC) simulator, such as that described by Flidr *et al.* (1998). This model incorporates the full structure of the Si(111) lattice, including the interlayer stacking pattern, and all possible reactive sites within the solid-on-solid approximation. Toroidal bounds are used to simulate an infinite surface. The etching simulations are started from a perfect miscut surface. Before the simulation begins a constant, site-specific etch rate is assigned to each type of site (e.g. terrace, monohydride step, dihydride step or kink). During the simulation, single atoms are randomly removed from the lattice subject to the desired site-specific etch rates. For the case of aqueous etching of silicon, diffusion of surface atoms and redeposition of etch products can be neglected, as these processes are known to be unimportant. After a short period of transient behaviour (the length of which depends on the simulation size), the simulated surface morphology reaches steady state and is independent of the starting conditions.

Although KMC simulations are relatively straightforward to implement, some care needs to be taken in the choice of algorithm. As we shall discuss in later sections, quantitative measurements require relatively large simulation sizes, typically a few thousand square ångströms in extent. To reach steady state, at least five to ten monolayers must be etched away. To avoid a computational bottleneck, the n-fold

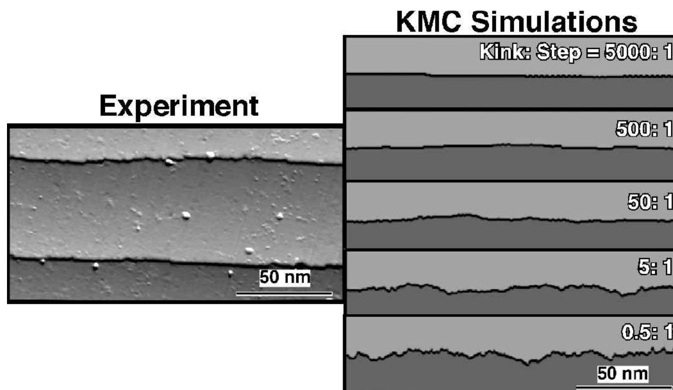

Figure 3. The roughness of etched steps reflects the anisotropic etching of kink and step sites. On the left, the STM image shows a Si(111) surface miscut by 0.3° in the $\langle 11\bar{2} \rangle$ direction and etched in 40% NH_4F(aq) for 60 min in a N_2 ambient. The five images on the right are KMC simulations with various kink:step etch rate ratios. Note the similarity between the experimental image and the 500:1 simulation.

Downloaded At: 16:40 21 January 2011

method of Monte Carlo simulation, which was first described by Bortz *et al.* (1975), is preferred.

To illustrate the interplay between experiment and simulation, figure 3 shows five different simulations of the etching of a single step edge. In these simulations, only two reactions were allowed: kink etching (etching across the step) and step etching (etching into the step). The final morphology is dependent on the anisotropy, the ratio of the kink to step etch rates. When the anisotropy is high and kink etching is very fast, the etched step is essentially straight. On the other hand, when the rates are nearly equal, the etched step has a very rough morphology.

By comparing simulated morphologies with those obtained experimentally, an estimate of the actual step-to-kink anisotropy can be obtained. For example, figure 3 also shows the morphology of a single step etched in 40% NH_4F. Based on this image, we can tentatively conclude that the kink site is more reactive than the step site by a factor of approximately 100. (Of course, firm conclusions cannot be drawn from a single experimental image.)

In this example, both the simulated and the experimental images were obtained from surfaces miscut in the $\langle 11\bar{2} \rangle$ direction. Thus, the step site corresponds to the monohydride-terminated step depicted in figure 2. These data provide essentially no information about the reactivity of the other type of step site, the dihydride-terminated site. This deficiency could be addressed by etching surfaces miscut towards the $\langle \bar{1}\bar{1}2 \rangle$ direction under the same experimental conditions, which would yield an estimate of the dihydride step-to-kink anisotropy.

2.2. *Etch pits and islands*

Vicinal steps are not the only morphological marker of etchant anisotropy. As mentioned earlier, the shape of etch pits (and islands) also provides information on etchant anisotropy. When a convex object, such as an island or sphere, is etched, the steady state etch form is composed of the *fastest*-etching steps or planes. In contrast, when a concave object, such as an etch pit or convex hollow, is etched, the steady state geometry expresses the *slowest*-etching steps or planes. The complementary

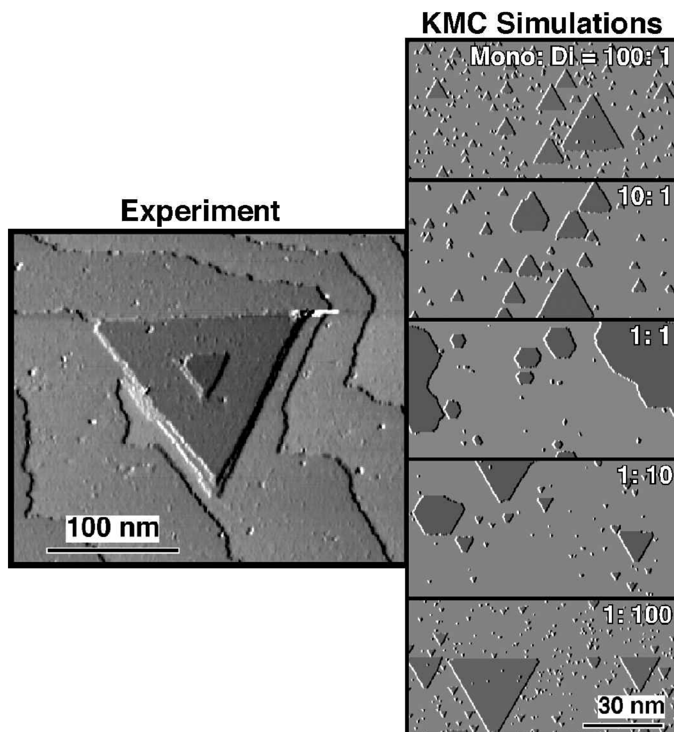

Figure 4. The shape of etch pits reflects the anisotropic etching of the two types of step. On the left, the STM image shows a Si(111) surface miscut by 0.3° in the $\langle\bar{1}\bar{1}2\rangle$ direction and etched in 40% $NH_4F(aq)$ for 60 min in a N_2 ambient. The five images on the right are KMC simulations with various monohydride step:dihydride step etch rate ratios. Note the similarity between the experimental image and the 1:100 simulation.

Downloaded At: 16:40 21 January 2011

nature of concave and convex etch shapes was elegantly demonstrated by Batterman (1957) in his study of etched germanium spheres and hollows. These shapes are also incontrovertible proof of the *non-equilibrium nature* of chemical etching, since the sphere and the spherical hollow had different limiting structures. In thermodynamic equilibrium, of course, both the sphere and the spherical hollow would express the same low-energy faces.

Figure 4 shows a particularly striking example of etch pit morphology. The three concentric etch pits in this image were propably generated by a defect, such as an oxide inclusion, in the original silicon wafer. The triangular shape of the pits is, however, completely due to the anisotropy of the etchant. All three pits are nearly perfect equilateral triangles, although close examination shows that some of the corners are slightly squared off.

Again, the chemical origins of these pits can be quantified with the aid of KMC simulations, such as the five simulations that are also shown in figure 4. (The simulated pits were generated by setting the rate of terrace etching to a small but finite value.) In the simulations, the relative etch rates of the two types of step were varied. When the two types of step etched with identical rates, amorphous or vaguely hexagonal pits were produced. In contrast, when one type of step etched more

rapidly than the other type, triangles were produced. The orientation of the triangles (up versus down) reflects the identity of the slow-etching step, whereas the perfection of the triangle is a measure of the anisotropy; high anisotropy gives nearly perfect triangles, whereas low anisotropy leads to blunted triangles.

By comparing the morphologies of experimental and simulated etch pits, the relative etch rates of the different step types can be estimated. In the case of 40% NH_4F etching, the images in figure 4 suggest that the strained dihydride-terminated step etches approximately 100 times more rapidly than the unstrained monohydride step.

These images also highlight the limitations of this single-feature approach to the quantification of etch morphologies. First, even in simulation, the features show some variability. In particular, statistical fluctuations lead to a significant variation in the morphology of small etch pits. Because of this, any quantitative analysis must be based on comparisons of many experimental and simulated images. Second, each type of morphological feature is only sensitive to changes in etchant anisotropy over a limited range. For example, a step anisotropy of 100:1 generates pits that are nearly indistinguishable from an etchant with a 1000:1 step anisotropy. Although the subtle difference between these two etchants could theoretically be resolved on an exceptionally large etch pit, pits of an arbitrary size may be difficult or impossible to generate.

In principle, etch islands should provide a second independent means of quantifying step anisotropy; however, not all etchants form both pits and islands. In principle, all etchants with a non-zero rate of terrace etching will form etch pits. When these etch pits coalesce, simple geometry dictates that islands must be formed at least some percentage of the time. In practice, the density of etch pits and thus the probability of pit coalescence are usually limited by the low density of vicinal steps found on even the best surfaces, since an etching step engulfs and removes any single-layer-deep etch pits in its path. At the present time, commercial silicon vendors can only cut and polish wafers with an orientational tolerance of $\pm 0.1^\circ$. (Even if a wafer were cut exactly parallel to a close-packed plane, imperfections in surface polishing would lead to pseudovicinal steps.) On Si(111), a miscut of 0.1° corresponds to a step–step distance of about 200 nm.

In fairness, it should be noted that the study of etchant anisotropy from etch pit morphology predates the invention of the scanning tunnelling microscope by many decades. In many systems, etch pits are rapidly nucleated wherever a dislocation intersects a surface. If the rate of etch pit nucleation is much faster than the rate of surface etching, a macroscopic etch pit will form around each dislocation. For the specific case of NH_4F/Si(111) etching, Huang (2000) showed that macroscopic dislocation-nucleated etch pits have the same shape as their atomic-scale brethren.

2.3. *More complicated features: etch hillocks*

Although all surfaces have steps, kinks and terrace sites, many surfaces have more exotic reactive sites as well. The presence of additional sites may lead to the production of more complicated etch structures, such as two-dimensional etch hillocks. The spontaneous formation of three-dimensional hillocks (convex, sometimes crystallographic features that form on an otherwise planar surface during etching or growth) has long puzzled engineers. Heterogeneous mechanisms for hillock formation are easily envisioned. For example, a piece of dust on an etching surface may lead to local surface masking and subsequent hillock formation. The

Downloaded At: 16:40 21 January 2011

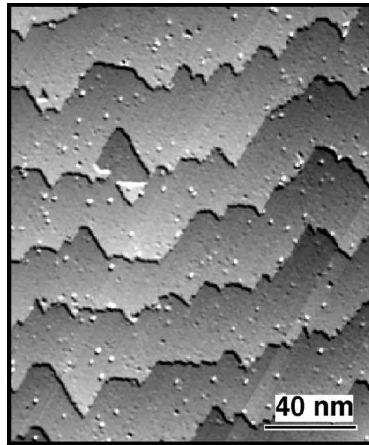

Figure 5. A STM image of a Si(111) surface miscut by 0.3° towards the $\langle\bar{1}\bar{1}2\rangle$ direction and etched in 40% NH_4F(aq) shows the development of two-dimensional etch hillocks which resemble shark's teeth.

Downloaded At: 16:40 21 January 2011

homogeneous nucleation of hillocks has long been suspected; however, a homogeneous mechanism for hillock formation is much harder to envision. Using a combination of STM and KMC simulations, Flidr *et al.* (1999) have shown that, under the appropriate conditions, a complex step geometry can lead to the spontaneous development of two- and three-dimensional hillocks.

The NH_4F-etched silicon surface in figure 5 shows an example of two-dimensional etch hillocks. Even though this surface was etched under the same reaction conditions that generated the nearly straight steps in figure 3, the etched steps in this image have an almost facetted appearance. After etching, the steps are decorated with many triangular shark's-tooth-shaped protrusions. The only difference between the surfaces in figures 3 and 5 is the orientation of this miscut. The surface in figure 3 was miscut towards the $\langle 11\bar{2}\rangle$ direction and has monohydride-terminated steps, whereas the surface in figure 5 was miscut towards the $\langle\bar{1}\bar{1}2\rangle$ direction. Because of this, the straight regions of step that are parallel to the macroscopic miscut direction are terminated by vertical dihydride units, while the straight sides of the sharks's teeth are monohydride-terminated steps. A statistical analysis of this morphology shows that only one third of the etched step sites have their expected dihydride-terminated configuration. The other two thirds of the step has spontaneously reoriented to form monohydride-terminated steps!

Although the steps in figure 5 appear to be facetted, they are not. Facetting is an equilibrium phenomenon that is driven by orientation-dependent differences in surface free energy. These structures cannot be explained by step pinning either, as the shark's-tooth shaped features have a characteristic size and shape. Pinned steps, in contrast, will elongate until the pinning site is removed. The shark's-tooth shaped features are two-dimensional etch hillocks—self-propagating features of a characteristic size and shape that travel with the etching step.

The formation of etch hillocks cannot be explained by simple step-and-kink etching. At least one more reactive species is necessary. Up to this point in our discussion, we have assumed that the two types of Si(111) step each have a single possible geometry. In fact, both steps have *two* possible geometries. For example, if

one row of silicon atoms were removed from the monohydride-terminated step sketched in figure 2, a trihydride-terminated step would be generated. The absence of a corresponding absorption band in the infrared spectrum of NH_4F-etched silicon surfaces does not rule out the existence of the trihydride. Instead, it merely suggests that the trihydride must be a very reactive species. Etching of a trihydride-terminated step would simply regenerate the stable monohydride termination actually observed in infrared studies.

The dihydride-terminated step also has two possible terminations. If a single row of silicon atoms were removed from the dihydride-terminated step shown in figure 2, a step terminated by a row of horizontal dihydride units would result. Since the horizontal dihydride is not observed in infrared studies, Jakob and Chabal (1991) assumed that steric interactions between neighbouring horizontal dihydrides destabilize this structure and lead to rapid etching. As with the other step orientation, if one row of silicon atoms were removed from a horizontal dihydride-terminated step, a new step, this time terminated by vertical dihydride units, would be formed.

If these two unstable step sites, the horizontal dihydride and the trihydride sites, were much more reactive than all other sites on the surface, these additional sites would have essentially no effect on the etch morphology. Once formed, the unstable step sites would be immediately etched away. The situation is more complicated when their reactivity is comparable with other species on the surface.

The first clue to the formation of etch hillocks is the very straight step edges in figure 5. Since extended regions of both monohydride- and dihydride-terminated steps are observed, we can immediately conclude that the kink sites etch much more quickly than either type of step site. (On Si(111), all kink sites have the same structure, regardless of the step termination.) This observation leaves one site unaccounted for, however, namely the site on the apex of the hillock. Since this site has the same crystallographic orientation as the vertical dihydride site, it can only be the previously unobserved *horizontal dihydride*. Although a step terminated by a row of horizontal dihydride units would be severely destabilized by the strong steric interactions between hydrogen atoms on neighbouring dihydride units, a single horizontal dihydride at the apex of a hillock would have no such steric hindrance. The presumed atomic structure of a horizontal-dihydride terminated etch hillock is shown in figure 6.

To investigate the role of this second step termination on etching, we modified our original KMC simulation to allow for two possible horizontal dihydride species with different etch rates: sterically unhindered isolated horizontal dihydrides or *point sites* as well as sterically hindered *adjacent* horizontal dihydride sites. Using kink, vertical dihydride step and monohydride step etch rates chosen to mimic the observed step and etch pit morphologies, we modelled the etching of surfaces miscut in the $\langle\bar{1}\bar{1}2\rangle$ direction with various point site etch rates. (Because of the severe steric hindrance, an infinitely fast etch rate for adjacent horizontal dihydrides was assumed.) The results of these simulations are shown in figure 7.

When the rate of point site etching is very fast ($k_{\rm pnt} > 0.1k_{\rm kink}$), the point sites have relatively little effect on the etched step morphology. Under these conditions, the etched step remains moderately straight, and its morphology is governed by the relative rates of kink and vertical dihydride step etching. If the rate of point site etching is decreased past this value, hillocks begin to form on the etching step, as shown in figure 7. The hillocks grow larger and more numerous until $k_{\rm pnt} \approx 0.025k_{\rm kink}$. Further stabilization of the point site has essentially no effect on

Downloaded At: 16:40 21 January 2011

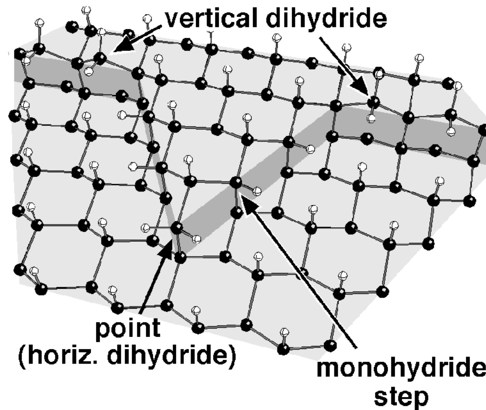

Figure 6. The atomic structure of a two-dimensional etch hillock on a surface miscut towards the $\langle\bar{1}\bar{1}2\rangle$ direction. The dark spheres represent silicon atoms, while the light spheres represent hydrogen atoms.

Downloaded At: 16:40 21 January 2011

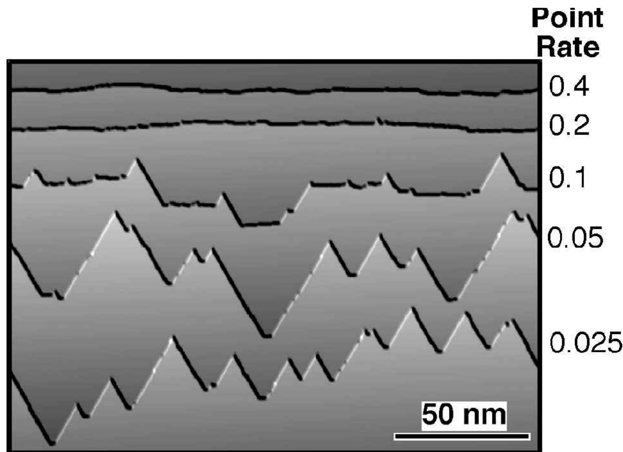

Figure 7. Simulated etch morphologies for $\langle\bar{1}\bar{1}2\rangle$ step etching using various point etch rates. In these, $k_{\text{kink}} = 1$, $k_{\text{vDi}} = 10^{-2}$, $k_{\text{Mono}} = 5 \times 10^{-4}$ and $k_{\text{terr}} = 0$.

step morphology, illustrating once again the limited range over which kinetically driven morphological changes occur.

The static images in figure 7 belie the elegance and complexity of the hillock formation process. Hillocks are not static features; they propagate across the surface with the etching step. To illustrate this, figure 8 shows a time lapse sequence of the evolution of a single etching step. Larger hillocks are seen to propagate with the step edge, while smaller hillocks are both created and destroyed in the course of the simulation. While propagating, the apices of the hillocks also undergo a random walk in the direction parallel to the step edge. A QuickTime movie of this process can be viewed at < http://www.chem.cornell.edu/mah11 > .

Hillock propagation is the result of a delicate kinetic balance between growth and decay, as illustrated by figure 9. Hillock growth is initiated by the etching of a vertical dihydride step, which produces two kink sites on the step adjacent to the hillock. Rapid kink etching subsequently removes an entire row of atoms from the

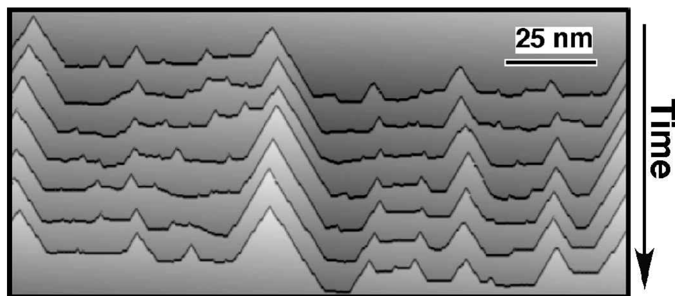

Figure 8. The time-dependent morphology of a single $\langle\bar{1}\bar{1}2\rangle$ step showing self-propagation of the two-dimensional hillocks.

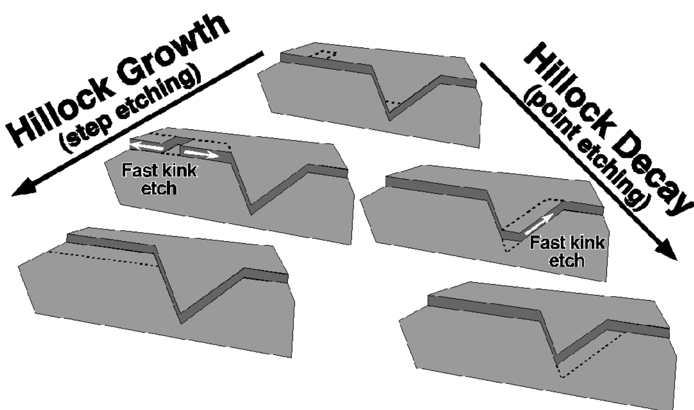

Figure 9. Hillock size is determined by the balance between growth and decay.

Downloaded At: 16:40 21 January 2011

step edge and effectively increases the hillock height by one unit. In contrast, hillock decay is initiated by the etching of the point site, which also generates two kink sites. (Detailed structural sketches of this process have been given by Flidr *et al.* (1999).) Rapid kink etching leads to the unzipping of one side of the hillock, which decreases the hillock height by one unit, and regeneration of the point site at a position one unit back from the original point.

The mean size of the etch hillocks is determined primarily by this kinetic balance between growth and decay. If an extended region of step contains N_{vDi} vertical dihydride sites with etch rate k_{vDi}, N_{mono} monohydride step sites with etch rate k_{mono} and N_{pnt} point sites, the balance between hillock growth and decay can be expressed mathematically as

$$N_{\mathrm{vDi}}\,k_{\mathrm{vDi}} = N_{\mathrm{pnt}}\,k_{\mathrm{pnt}} + N_{\mathrm{mono}}\,k_{\mathrm{mono}}. \tag{1}$$

In the case of NH_4F etching, where the rate of vertical dihydride step etching is significantly faster than the rate of monohydride step etching, this equation can be rearranged to estimate the actual rate of point site etching:

$$k_{\mathrm{pnt}} \approx \frac{N_{\mathrm{vDi}}}{N_{\mathrm{pnt}}} k_{\mathrm{vDi}}. \tag{2}$$

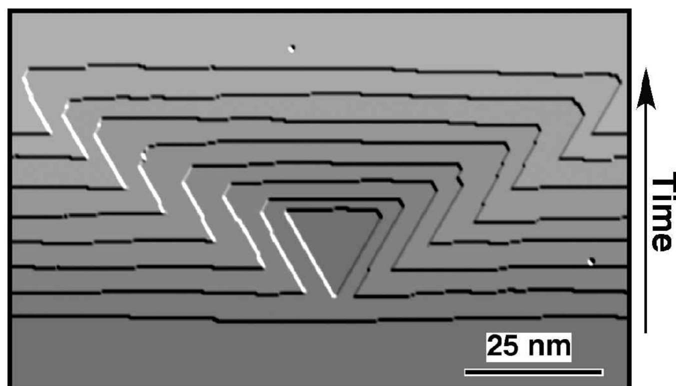

Figure 10. The time-dependent morphology of a $\langle 11\bar{2}\rangle$ step. After the step collides with a pit, two unstable hillocks are nucleated. The centrelines of these hillocks are oriented $\pm 60°$ from the step normal. The hillocks propagate along their centrelines.

Downloaded At: 16:40 21 January 2011

From a statistical analysis of etched surfaces like that in figure 5, equation (2) can be used to show that the point site etches approximately three times more rapidly than the vertical dihydride site. In other words, the unstrained dihydride is *significantly more reactive* than the strained dihydride. The chemical implications of this observation will be discussed in section 3.2.

In addition to these stable hillocks, unstable hillocks can also be nucleated on monohydride-terminated steps (i.e. on surfaces miscut towards the $\langle 11\bar{2}\rangle$ direction) by step–pit collisions. This process is illustrated by the time lapse sequence of a single etching step shown in figure 10. Initially, the etching surface consists of a relatively straight monohydride-terminated step and a single 200 Å triangular etch pit. When the step and pit collide, two unstable hillocks are nucleated at the point of collision. In contrast with the previous case, the centreline of these hillocks is rotated by $\pm 60°$ from the step normal. Further etching causes these hillocks to propagate away from their original position, along the hillock centreline. In contrast with stable hillocks on vertical dihydride steps, these unstable hillocks are not bounded by vertical dihydride steps. Because of this, hillock growth is impossible, and the hillocks gradually decay in size.

These unstable hillocks produce 'pit scars' in monohydride-terminated steps. These scars can be deceiving, however, because the scars are often much larger than the original pits. For example, the width of the scar in figure 10 grows by a factor of about seven over the course of the simulation, while the height only decreases by 25%. Because of this effect, small pits can lead to large scars and pronounced step meandering.

The growth of pit scars with etching illustrates an important point. Although casual observation can often yield a reasonable *qualitative* understanding of etchant anisotropy, full atomistic simulations are often needed for a complete understanding. The shapes of individual etch features are easily distinguished by eye, but the interactions between the various features can be deceptively complex. For example, the presence of large pit scars does not imply the previous existence of large etch pits. In fact, pit scars are not a general result of pit–step collisions. Unless a stable (slow etching) species such as the point site terminates the pit scar, subsequent etching will quickly round the edges of the scar and remove all traces of its presence.

2.4. *Setting the scale with interacting etch features*

In the previous sections, we discussed the effects of site-specific etching on individual surface features and showed that the shape of each feature can be attributed to the relative etch rates of two or more sites. From this discussion, one might assume that a complete set of etch rates could be extracted from the observation of a few individual features; however, this is not the case! In particular, the rate of terrace site etching cannot be related to any other rate using single feature analysis. More importantly, the propagation of uncertainties in a sequential analysis limits the utility of this approach.

During etching, individual etch features interact with and are influenced by one another. For example, etch pits can collide with passing steps and be engulfed. Because of this interaction, the characteristic size and density of etch pits is determined by both the terrace etch rate (i.e. the rate of pit nucleation) and the density of vicinal steps (i.e. the rate of pit decay). This relationship is illustrated by the simulations in figure 11. All these simulations were performed with exactly the same site-specific kinetics; the only difference between the simulations is the step density. At low step densities, the pit density is high, because the pits have a long time to nucleate between passing steps. As the step density increases, both the pit density and the average pit size decrease. Perhaps more importantly, the step morphology is also very sensitive to the surface miscut. Low step densities increase the importance of step–pit interactions, thereby increasing step meandering.

Downloaded At: 16:40 21 January 2011

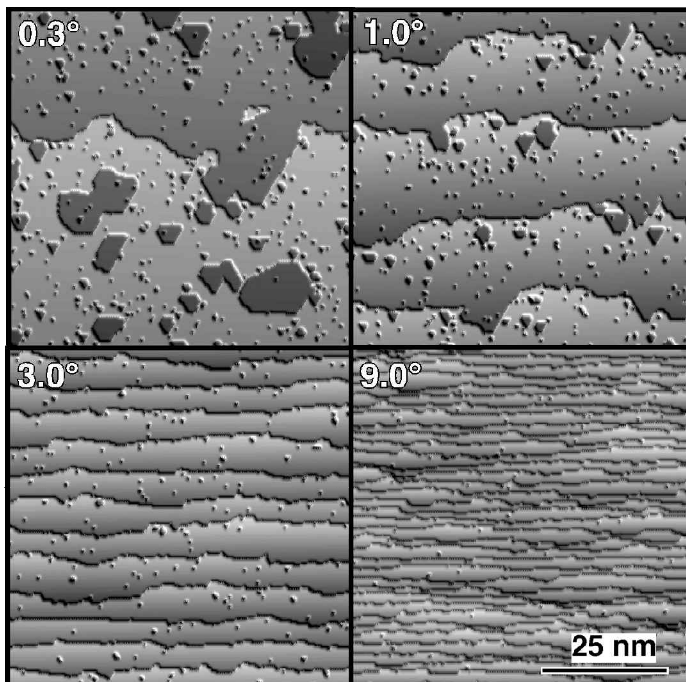

Figure 11. The step density controls the size and density of etch pits as well as the etched step morphology. All four of these KMC simulations were generated with identical site-specific etch rates. The only difference between the simulations is the magnitude of the miscut.

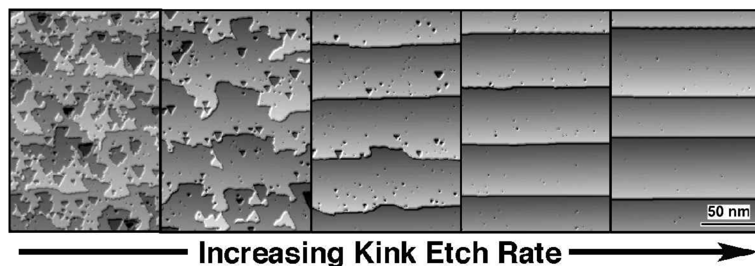

Figure 12. The etched surface morphology is very sensitive to interactions between various morphological features. In these simulations, all the etch rates were identical *except* for the kink etch rates. Since the kink rate controls both step straightness and the rate of step etching, step–pit interactions are influenced by this rate.

Downloaded At: 16:40 21 January 2011

More complicated interactions are also possible. For example, figure 12 shows five nearly identical simulations. The only variable that was changed between the simulations was the rate of kink etching. When the rate of kink site etching was very high, the etched steps were very straight, as expected from the discussion in section 2.1. As the kink etch rate was lowered, both the steps and the surfaces became rougher and rougher. This roughness was primarily due to pit–step collisions and not to the inherent roughness of the etched steps. As the rate of kink site etching was lowered, the overall rate of step etching also decreased. Of course, when the steps move more slowly, the etch pits have more time to nucleate and grow. Because of this, step–pit collisions are much more frequent at low kink rates, and they play a correspondingly larger role in determining the etch morphology.

The simulations in figures 11 and 12 illustrate the important role that vicinal steps play in 'setting the scale' of anisotropic etching. Since etching steps erase features in their path and uncover new regions of fresh unetched surface, a known step density serves as an absolute clock against which the size and density of other features can be compared.

This observation has three important implications. First, experimental investigations of etchant anisotropy should be performed on surfaces with a non-zero miscut of known orientation. The miscut angle determines the step density, while the miscut orientation determines the step geometry. Second, the step density should be chosen to match the etchant anisotropy. Etchants with slow pit nucleation and fast step etching are best studied on low-step-density surfaces, because these surfaces allow ample time for pit nucleation and growth. For example, most of our studies of NH_4F etching were performed on surfaces miscut by a mere 0.35°. In contrast, etchants that display facile pit nucleation should be studied on highly miscut surfaces. Otherwise, pit–step collisions will rapidly obscure the structure of the vicinal steps. Finally and perhaps most importantly, *quantitative comparisons of experimental and simulated surface morphologies can only be performed on identically scaled images*. Failure to follow this simple rule can lead to errors of many orders of magnitude in the measured site-specific etch rates!

Of course, the analysis of etch morphologies must be performed on a statistically significant number of experimental images and simulations. A single arbitrary image can be extremely misleading. In fact, T. P. Beebe, Jr (1995, private communication) once observed an etch pit on graphite that bore a striking resemblance to a dancing elephant!

3. Extreme anisotropy: the etching of silicon by NH_4F

The previous section dealt with the various 'clues' that one can obtain from a visual inspection of an etched surface. Many of these clues were illustrated with examples drawn from our studies of Si(111) etching in 40% NH_4F(aq). In this section, we shall first concentrate on the general issue of *quantification* of site-specific etch rates. Following this, we shall discuss the specific chemistry that governs the etching of silicon by NH_4F, an extremely anisotropic etchant.

The first question that everyone asks is why study Si(111)? After all, the microelectronics industry revolves around the (100) surface, and so Si(100) wafers are much cheaper and more readily available. The answer lies in the structure of the (111) surface. From a chemist's perspective, the Si(111) surface is nearly ideal, because this surface has a large number of chemically distinct sites that have been previously characterized by detailed spectroscopic studies. This surface has two distinct monohydride species (terrace and kink), three distinct dihydride species (vertical dihydride and isolated and adjacent horizontal dihydrides) and a trihydride species. At least in principle, a study of Si(111) etching should lead to chemical insights that are applicable to any silicon surface.

Having decided on the surface to study, which experiments should be performed? Since Si(111) has two principle miscuts, it is imperative that both miscuts be studied. If the angles of the miscuts are chosen correctly, little additional information will be garnered from a study of (nominally) flat surfaces. Since NH_4F is a highly anisotropic etchant, we chose a very low surface miscut. A few wafer vendors, including Virginia Semiconductor, can supply precision miscut wafers with a tolerance of $\pm 0.1°$. With this tolerance in mind, we chose a 0.35° miscut, which corresponds to a step–step spacing of about 50 nm.

As we shall discuss in more detail later, silicon etching is extraordinarily sensitive to contaminants of all types. Because of this, the most important step in every experiment is cleaning! Before every experiment, all the laboratoryware and the silicon sample are cleaned using a procedure based on the original RCA clean developed by Kern and Puotinen (1970). An excellent review of silicon cleaning procedures and their chemistries has been given by Higashi and Chabal (1993). Prior to etching, the laboratoryware, which must be either glass or solid Teflon (no metal!), is cleaned in a basic peroxide solution (SCA-1), which is composed of 1:1:4 by volume of 28% NH_3(aq):30% H_2O_2(aq):H_2O at 80°C, for at least 10 min and then rinsed thoroughly in running ultrapure water (Millipore Milli-Q). The sample is then cleaned in a fresh SCA-1 bath (in a pre-cleaned beaker) for 10 min. The oxide layer is stripped with a 2 min immersion in an aqueous HF/NH_4F solution (Buffer-HF, Transene). After a thorough rinsing, the sample will be hydrogen terminated, as evidenced by its pronounced hydrophobicity. To ensure cleanliness, a second SCA-1 cleaning and HF strip are performed. Following this, a SCA-2 clean is optionally performed to remove possible metal contamination. In this procedure, the hydrogen-terminated surface is cleaned in a 1:1:4 bath of 37% HCl(aq):30% H_2O_2(aq):H_2O for 10 min at 80°C and rinsed in flowing ultrapure water.

The studied morphologies were completely determined by the final processing step: a 30 min etch in a stirred room-temperature 40% NH_4F(aq) solution (Transene) in an ambient atmosphere. Experimentally, we found that the surface morphology reached steady state in this time. After etching, the sample was rinsed by a 20 s dip in ultrapure water. An InGa Ohmic contact was then applied to the back

Downloaded At: 16:40 21 January 2011

side of the sample, and the surface was loaded into a load-locked ultrahigh-vacuum (UHV) scanning tunnelling electron microscope for analysis. A UHV scanning tunnelling microscope has two distinct advantages over an atmospheric scanning tunnelling microscope. First, the etched hydrogen-terminated surface is only oxidation resistant for a matter of hours in an ambient atmosphere, but it is stable indefinitely in UHV. Since the cleaning and etching procedure requires about 2 h of preparation, an UHV instrument is much more convenient for extended imaging. Second, UHV instruments can use tungsten tips, which are considerably more robust and reliable than the Pt–Ir tips used in air. *In-situ* tip processing procedures can also be performed in UHV to rescue a dull tip. We have avoided *in-situ* imaging because of concerns about constrained diffusion in the vicinity of the scanning tunnelling microscope tip, electron-induced chemistry and contamination.

Once a large sample of etched surface morphologies have been compiled from surfaces miscut in both the $\langle 11\bar{2}\rangle$ and the $\langle \bar{1}\bar{1}2\rangle$ directions, the site-specific etch rates can be extracted by direct comparison with KMC simulations. A visual examination of the morphologies is used to generate a zeroth-order set of site-specific etch rates, and then this set is refined through an iterative trial-and-error process. Although we have experimented with many mathematical parametrizations of surface morphology (e.g. height–height correlation functions (Tong and Williams 1994)), the quality of fit is best judged by eye. (For studies of long-range surface morphology, the terrace width distribution can also be valuable, as shown by Huang *et al.* (1998a).) Both the simulations and the experiments should be performed on surfaces with identical miscuts, and the images should contain at least two to four vicinal steps. Particular attention should be paid to the step edge morphology, and the size, density and shape of etch pits, as well as any other characteristic features (e.g. hillocks and islands). Images obtained near the edge of the sample may contain defect-related etch pits and should thus be avoided.

Downloaded At: 16:40 21 January 2011

3.1. *Site-specific rates and chemical mechanism*

Like most aqueous etchants, NH_4F continuously removes silicon through sequential oxidation and etching reactions. Newton (2000) showed that the rate of NH_4F etching is linearly dependent on $[OH^-]$ and independent of fluorine concentration, at least in the concentration range appropriate to 40% NH_4F. From this, the reactions are assumed to be

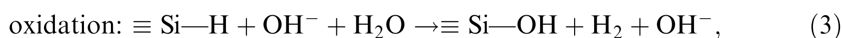

$$\text{oxidation: } \equiv \text{Si—H} + \text{OH}^- + \text{H}_2\text{O} \rightarrow \equiv \text{Si—OH} + \text{H}_2 + \text{OH}^-, \tag{3}$$

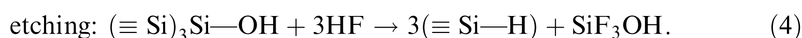

$$\text{etching: } (\equiv \text{Si})_3\text{Si—OH} + 3\text{HF} \rightarrow 3(\equiv \text{Si—H}) + \text{SiF}_3\text{OH}. \tag{4}$$

Since the etched surface is profoundly hydrogen-terminated (Higashi *et al.* 1990), oxidation is the rate-limiting step, and the steady-state surface morphology is determined by the site specificity of the rate limiting reaction (3).

Figure 13 shows representative experimental and simulated images of Si(111) etched in 40% $NH_4F(aq)$. Both simulations were performed with the same set of site-specific etch rates; the only difference between the simulations is the orientation of the surface miscut. From these simulations, the relative site-specific etch rates were determined to be as follows: kink, 1; point, 0.1; vertical dihydride (step), 0.01; monohydride (step), 0.005; terrace, 10^{-7}. (The trihydride and adjacent horizontal dihydride are too reactive to be measured by this technique, so their rates were assumed to be infinitely fast.) The simulated morphologies are very sensitive to

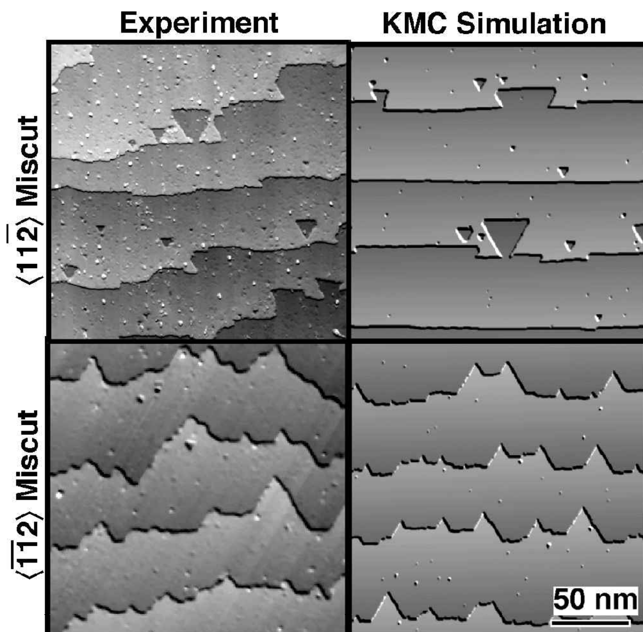

Figure 13. A comparison of the experimental and simulated morphologies of Si(111) surfaces miscut by 0.3° and etched in stirred NH_4F(aq). Surfaces miscut in the ⟨11$\bar{2}$⟩ direction show unstable etch hillocks (pit scars), while surfaces miscut in the ⟨$\bar{1}\bar{1}$2⟩ direction show stable etch hillocks. The KMC simulations are the best fit to experiment. In these, $k_{\mathrm{kink}} = 1$, $k_{\mathrm{vDi}} = 10^{-2}$, $k_{\mathrm{Mono}} = 5 \times 10^{-4}$, $k_{\mathrm{terr}} = 10^{-7}$ and $k_{\mathrm{pnt}} = 0.10$.

Downloaded At: 16:40 21 January 2011

changes in these rates. Although varying any one rate by a factor of two to three results in only minor morphological changes, larger changes or changes in multiple rates lead to degradation of the simulations. Interestingly, even though all the surface sites are silicon hydrides, the site-specific reactivities span a huge range; the strained and distorted kink site is 10^7 times more reactive than the flat terrace site!

The correlation between the structure and reactivity of the sites provides important information about the nature of the reaction mechanism. In this case, there are two highly strained sites (kink and vertical dihydride) and three unstrained sites. Although there is a rough correlation between strain and reactivity, *strain cannot fully explain the observed reactivities*. Instead, the observed reactivities can be explained by the existence of a pentacoordinate transition state to hydrogen displacement as postulated by Hines *et al.* (1994). In organosilicon chemistry, similar nucleophilic displacements of hydrogen by OH^- have been observed, and these reactions are believed to proceed through bimolecular, front-sided attack (Rochow 1973, Armitage 1982). In addition, many pentacoordinate silicon anions have been observed and characterized (Hajdasz and Squires 1986, Holmes 1990). As a result, silicon sites that are held in a rigid tetrahedral environment react much more slowly than those held in less rigid or in distorted environments.

The proposed pentacoordinate transition state explains the reactivity of *all* the sites. Sites that are held in a rigid tetrahedral geometry by three bonds to the silicon substrate are difficult to distort. As a result, terrace and monohydride step sites are

relatively unreactive. On the other hand, sites that are already in a near-pentacoordinate geometry, such as the kink site, are highly reactive. The vertical dihydride lies in between these two extremes. Although this site is highly strained by steric interactions, *ab initio* cluster models show that the silicon centre is nearly tetrahedral (Raghavachari *et al.* 1993). Because of this, the vertical dihydride is less reactive than the kink site, but more reactive than sites that are triply coordinated to the surface. In contrast, the point site, which is a horizontal dihydride, is unstrained. Because of this, both of the Si—H bonds are free to distort. As a result, the unstrained horizontal dihydride is actually *more reactive* than the strained and hindered vertical dihydride.

3.2. *Impurities and other sources of frustration*

Since Higashi *et al.* (1990) first reported the production of ultraflat Si(111) by NH_4F etching, STM studies of various aspects of this fascinating system have been reported by many groups, including Becker *et al.* (1990), Hessel *et al.* (1991), Pietsch *et al.* (1993), Hsiao *et al.* (1993), Kaji *et al.* (1995) and Wade and Chidsey (1997). To the outside observer, these papers might be confusing, because every paper seems to report a somewhat different morphology! Although most of the images in the literature are similar, there are also striking differences.

Although the hydrogen-terminated Si(111) surface is surprisingly resistant to oxidation in air, the etching surface is extremely sensitive to contamination! In particular, Wade and Chidsey (1997) showed that dissolved O_2 can nucleate etch pits. Surfaces etched in an argon-purged solution of NH_4F had a significantly lower density of pits than those etched in air-containing NH_4F. This effect was attributed to trace amounts of O_2^- which were presumed to react with the surface according to

$$O_2^- + \equiv \mathrm{Si{-}H} \rightarrow \equiv \mathrm{Si}\cdot \; + HO_2^- . \tag{5}$$

Additionally, Huang *et al.* (1998a) showed that the etch morphology is surprisingly sensitive to stirring. Surfaces etched in stirred NH_4F solutions have a very regular distribution of surface steps, while surfaces etched in unstirred solutions show step bunching. The regular step distribution is easily explained by dynamic step–step repulsion (Huang *et al.* 1998b), a rather esoteric topic that is beyond the scope of this review. Since the NH_4F reaction sequence is autocatalytic in OH^- (see reactions (3) and (4)), step bunching in unstirred solutions was tentatively attributed to localized autocatalysis. Presumably, stirring homogenizes the reactants and prevents this process.

Because of these two effects, the surface morphology is very sensitive to both the etching atmosphere and the stirring conditions. If large flat Si(111) terraces are desired, an unstirred solution works best. On the other hand, quantitative studies of etchant reactivity assume a constant concentration of reactants, so the solution must be well stirred.

Figure 14 shows the results of preliminary experiments designed to quantify the effects of dissolved O_2 on NH_4F etching. The three surfaces were miscut by 0.35° towards the $\langle 11\bar{2}\rangle$ direction and etched in identical stirred containers of NH_4F. The only difference between the images is the atmosphere: ultrapure N_2, air (18% O_2) and ultrapure O_2. Visual inspection shows that dissolved O_2 has two principal effects: it increases the rate of pitting (i.e. terrace nucleation) and it also decreases the anisotropy of the etch pits. Although data for the $\langle \bar{1}\bar{1}2\rangle$ miscut must be obtained for

Downloaded At: 16:40 21 January 2011

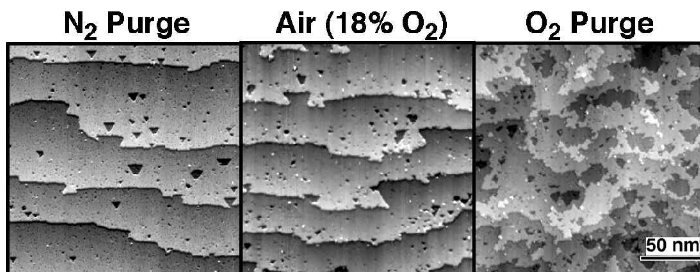

Figure 14. A comparison of three Si(111) surfaces miscut by 0.3° in the $\langle 11\bar{2} \rangle$ direction and etched in stirred NH_4F(aq). The solutions were maintained in a N_2 purge, ambient air (nominally 18% O_2) and an O_2 purge. The pit density and anisotropy are both affected by dissolved O_2.

a full analysis, preliminary simulations show that saturating an NH_4F solution with oxygen increases the terrace etch rate by a factor of about 30 and the monohydride step rate by a factor of about three compared with a N_2-purged solution. Although the etch rates of the other sites are essentially unaffected by O_2, the other sites also have a much higher etch rate in NH_4F. Clearly, the reactivities of NH_4F and dissolved O_2 towards silicon are very different.

Etched silicon surfaces are also subject to contamination by what appear to be 'white dots' in STM images. Since the dots can be moved with the STM tip, they correspond to some physisorbed material. Our experience shows white dots can be deposited during the final rinse, presumably when the surface is pulled through the air–water interface. The chemical composition of these dots is unknown; however, Y. J. Chabal (1994, private communication) has shown that hydrogen-terminated silicon surfaces are extremely susceptible to hydrocarbon contamination, especially during the load locking process. In fact, roughing the load lock chamber with a mechanical pump leads to instantaneous contamination of the hydrogen-terminated surface with a thick layer of hydrocarbons, as verified by *in-situ* Fourier transform infrared spectroscopy.

Finally, the hydrogen-terminated surface is also subject to damage by the STM tunnelling current; however, this problem can be avoided with the proper tunnelling conditions. Shen *et al.* (1995) have shown that electron-induced desorption of hydrogen occurs by two distinct mechanisms and have characterized their current–voltage dependences. Lyding *et al.* (1994) have used this effect to perform nanoscale patterning of hydrogen-terminated silicon.

4. Unravelling complexity with kinetic competition: the unusual effects of isopropanol on etching

In the previous section, we showed that an etched surface morphology can be analysed to reveal the site specificity of a simple anisotropic etchant, but many etchants are complex, containing two or more active components. In this section, we shall show how these techniques can be extended to allow for multicomponent analyses, even when one of the components does not etch the surface.

Because of their low cost and high reproducibility, aqueous silicon etchants are often used in the fabrication of microelectromechanical systems, such as the accelerometers that are used to trigger automobile airbags. After the desired

Downloaded At: 16:40 21 January 2011

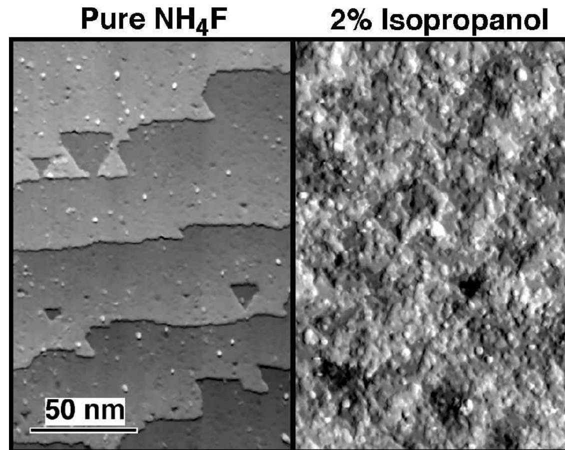

Figure 15. A comparison of two Si(111) surfaces miscut by 0.3° in the $\langle 11\bar{2} \rangle$ direction and etched in either stirred NH_4F(aq) or stirred NH_4F(aq) containing 2% IPA by weight.

Downloaded At: 16:40 21 January 2011

structure is defined and masked using lithographic processes, the chemical etchant is used to remove unwanted areas of silicon. The anisotropy of aqueous etchants has an undesirable side effect in machining, however: it causes the etchant to undercut some areas of the mask, particularly convex corners. To reduce this problem, a reputedly inactive chemical agent, isopropanol (IPA), is often added to the etchant. Not only does this additive reduce undercutting by up to 75% (Puers and Sansen 1990, Merlos *et al.* 1993), it also smooths the etched surface by preventing the formation of etch hillocks (Campbell *et al.* 1995). Recently, Wind and Hines (2000) have shown that IPA induces a dramatic change in the macroscopic anisotropy (i.e. the face specificity) of KOH(aq)/Si etching, as well as a marked decrease in the overall etch rate.

How does IPA effect these pronounced changes in etch morphology and etchant anisotropy? Interestingly, IPA does not etch silicon directly. In fact, spectroscopic studies by Palik *et al.* (1983) concluded that IPA does not even participate chemically in the etching reactions; however, recent STM experiments by Allongue (1996) have shown evidence of slow IPA binding in electrochemically driven systems. Because of this lack of evidence of direct chemical attack, the morphological effects of IPA have most often been attributed to reduced surface tension (Campbell *et al.* 1995) or reduced solvation of the etchant (Seidel *et al.* 1990).

In addition to its macroscopic effects, IPA also affects the etched surface morphology on the nanometre length scale. Figure 15 compares the morphology of a surface etched in pure NH_4F(aq) with a similar surface etched in NH_4F(aq) with 2% IPA added. From these images, it is apparent that IPA reduces the overall etchant anisotropy; however, the IPA-enhanced morphology raises an immediate question: how can this morphology be analysed? Instead of the easily analysed straight steps and triangular etch pits seen in NH_4F etching, the IPA-enhanced etchant produces a surface that resembles oatmeal!

Since IPA reduces the rate of silicon etching without etching the surface itself, it is logical to assume that IPA must be binding (in some fashion) to at least some sites on the etching surface and blocking their etching. This binding cannot be permanent, however, or the surface would develop etch hillocks under each blocked site. As a

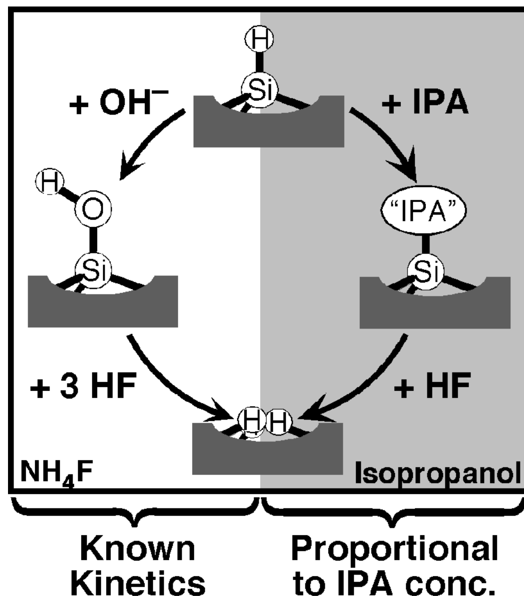

Figure 16. In solutions containing both NH_4F and IPA, two reaction channels are open to the etching surface. The relative importance of the two channels is controlled by the IPA concentration.

Downloaded At: 16:40 21 January 2011

result, IPA must be introducing at least two new site-specific reactions: the binding of IPA to a site and the removal of the IPA-bound species. The morphology of a surface etched in a mixture of NH_4F and IPA must be governed by four simultaneous reactions: the oxidation and etching of silicon by NH_4F (reactions (3) and (4)), and the binding and removal of IPA from the surface. These competing pathways are illustrated by figure 16.

4.1. *Concentration effects and kinetic competition*

Figure 16 implies that 28 rate constants, corresponding to four reactions at each of seven different reaction sites, must be known to model the morphology of IPA–NH_4F-etched silicon—a seemingly formidable challenge! Fortunately, these are competing reactions that can be analysed through their concentration dependence. The 14 rates of NH_4F etching can be quantified by etching surfaces in pure NH_4F as described earlier. Since reaction (3) is rate limiting, the site-specific rates of reaction (4) are irrelevant, and only seven site-specific rate constants are needed. The site-specific rates of the two remaining reactions can be inferred from a study of the IPA concentration dependence, as illustrated by figure 17. (Full experimental details have been given by Newton *et al.* (1999).)

The major trends in IPA reactivity can be inferred from a visual comparison of the etched surface morphologies obtained with different concentrations of IPA. For example, surfaces etched in 0.02% IPA solutions have larger pits than those etched in pure NH_4F. In this system, pit size is controlled by the rate of kink etching (Flidr *et al.* 1998). Since highly reactive kinks lead to rapid step advancement and correspondingly fast pit annihilation, the average pit size is inversely related to the kink etch rate. The increase in pit size upon IPA addition is indicative of

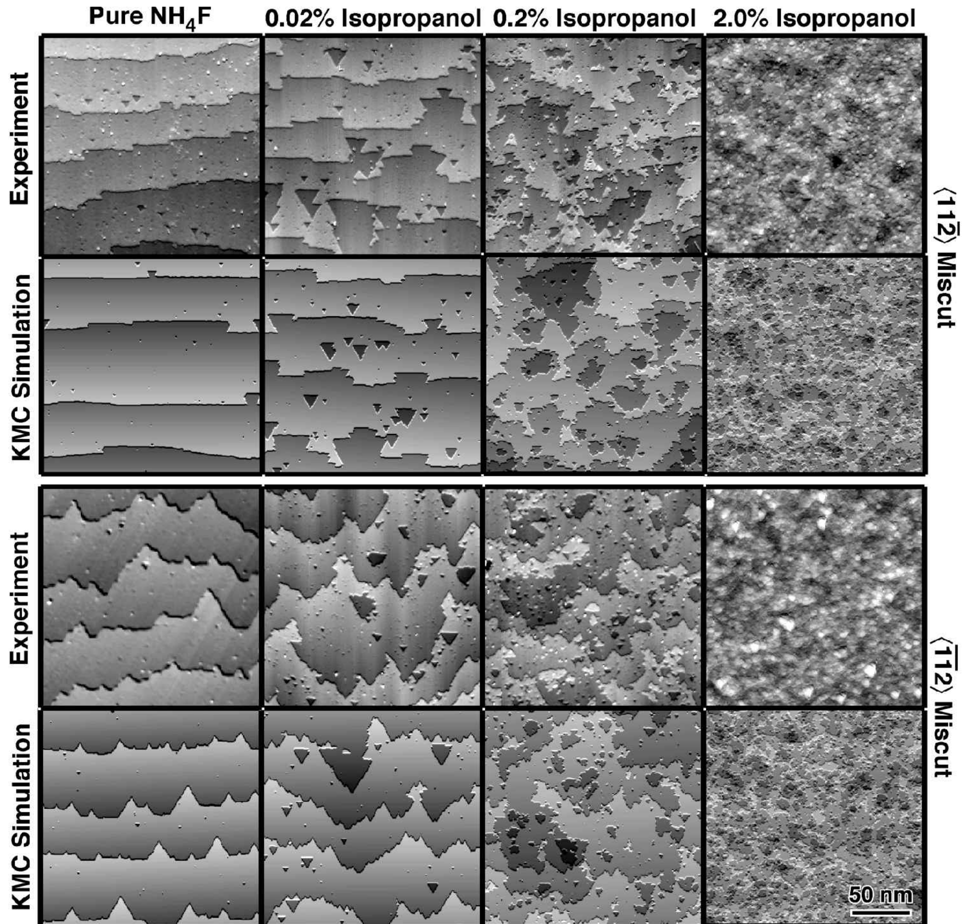

Figure 17. Observed and simulated steady state morphologies of Si(111) etched in IPA/ NH_4F solutions. All simulations used the same site-specific reaction rates (see table 1); only the initial miscut and IPA concentrations were changed. The surface miscut is towards the $\langle 11\bar{2}\rangle$ direction in the top two rows, and towards the $\langle \bar{1}\bar{1}2\rangle$ direction in the bottom two rows. The IPA concentration is indicated at the top of each column.

Downloaded At: 16:40 21 January 2011

selective IPA binding to kink sites. Thus, kink sites must be the most susceptible to IPA attack. When the IPA concentration is increased to 0.2%, the etch pits become very irregular. This loss of triangularity is due to reduced anisotropy in step etching. Since IPA lowers the overall etching rate, this loss of anisotropy must be due to selective binding of IPA to the fast etching steps, namely the vertical dihydride step sites. At the highest IPA concentration, step flow etching is quenched, and the surface etches in a very isotropic fashion. Although individual steps can still be imaged, the step edges are rough and crenulated. Under these conditions, all three step sites (kink, vertical dihydride and horizontal monohydride) appear to etch at approximately the same rates, which implies that IPA-contaminated step sites all etch with similar rates.

These trends can be quantified with KMC simulations. In the simulations, every site S on the surface can be terminated either by hydrogen (S_H) or by an IPA-related

Table 1. The site-specific rates of reactions (3), (9) and (10). In reaction (9), c denotes the percentage of IPA (e.g. $c = 2$ in 2% solutions).

Site	Site-specific rate			Strain
	NH_4F etching (reaction (3))	OR^- attack (reaction (9))	Si—OR etching (reaction (10))	
Kink	1	$1c$	4×10^{-5}	Yes
Point	0.1	$0.2c$	0.005	No
Di step	0.01	$0.05c$	4×10^{-5}	Yes
Mono step	0.0005	$0.0005c$	4×10^{-5}	No
Terrace	10^{-7}	0	—	No

species (S_{IPA}). The three possible reactions and their corresponding site-specific reaction rates are thus

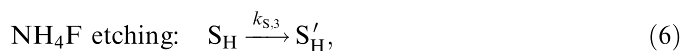

$$\text{NH}_4\text{F etching:} \quad S_H \xrightarrow{k_{S,3}} S'_H, \tag{6}$$

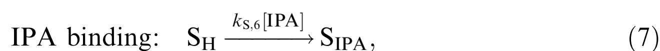

$$\text{IPA binding:} \quad S_H \xrightarrow{k_{S,6}[\text{IPA}]} S_{IPA}, \tag{7}$$

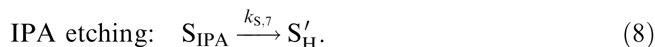

$$\text{IPA etching:} \quad S_{IPA} \xrightarrow{k_{S,7}} S'_H. \tag{8}$$

In the simulation, the rate of IPA binding, reaction (7), is assumed to be linearly dependent on the IPA concentration, while the other two reaction rates are assumed to be concentration independent. As before, the KMC simulations included the full structure of the Si(111) lattice and all possible reaction sites. During the simulation, single sites were allowed to react or etch subject to the site-specific rates of NH_4F etching (k_{S3}), IPA binding (k_{S6}[IPA]) and IPA-bound site etching (k_{S7}).

The site-specific rates of reactions (7) and (8) were adjusted until the best fit to the experimental morphologies was obtained. In judging the quality of the fit, particular attention was paid to morphological features that underwent a dramatic change between successive increases in IPA concentration (e.g. the pit sizes in 0.02% IPA, the pit shapes in 0.2% IPA and the disappearance of discernible vicinal steps in 2.0% IPA). The extracted site-specific reaction rates are given in table 1, and the corresponding simulated morphologies are displayed in figure 17. All the simulations were generated from the *same set of site-specific reactivities*; only the surface miscut and IPA concentration were varied. The simulated morphologies are very sensitive to changes in these rates. Although varying any one rate by a factor of two to three resulted in only minor morphological changes, larger changes or changes in multiple rates lead to degradation of the simulations. There are essentially no cross-correlations in the fit parameters (e.g. an increase in the kink etch rate cannot be compensated by a decrease in another etch rate).

4.2. *The mechanism of isopropanol*

The site-specific rates of IPA binding and etching provide key insights into the mechanism of IPA-induced morphological changes. For example, table 1 shows that

Downloaded At: 16:40 21 January 2011

the site-specific rates of OH^- attack and IPA binding are *highly correlated*, which strongly suggests that the reactions proceed through similar mechanisms.

In aqueous solutions, an alcohol HOR can dissociate to form an alkoxide ion OR^- and a proton H^+. Although this reaction is energetically unfavourable, alkoxide ions exist in significant concentrations. For example, the pK_a of isopropanol (17.1) (Serjeant and Dempsey 1979) implies that $[OCH(CH_3)_2^-] \approx 10^{-3}[OH^-]$ for 2% IPA solutions, regardless of pH. As one might expect, the reactivity of OR^- resembles that of OH^- in many respects. Nucleophilic displacement of hydrogen by alkoxide ions is well known in organosilicon chemistry (Corriu and Guerin 1982). Since this reaction proceeds through the same bimolecular, front-side attack mechanism as the OH^--mediated reaction, Newton *et al.* (1999) proposed that IPA reacts through the analogous sequential reactions

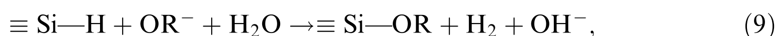

$$\equiv \text{Si—H} + OR^- + H_2O \rightarrow \equiv \text{Si—OR} + H_2 + OH^-, \tag{9}$$

$$(\equiv \text{Si})_3\text{Si—OR} + 3HF \rightarrow 3(\equiv \text{Si—H}) + SiF_3OR, \tag{10}$$

where $R = CH(CH_3)_2$. Bitzer *et al.* (1997) observed the surface isopropoxy species in UHV silicon reactions and characterized this species by vibrational spectroscopy.

If the isopropanol reaction resembles the NH_4F reaction, why are the etched surface morphologies so sensitive to IPA concentration? The answer lies in the relatively slow rate of the silicon isopropoxy etching reaction (10). In contrast with NH_4F etching where oxidation (reaction (3)) is rate limiting, the rate of silicon isopropoxy etching (reaction (10)) is much slower than the rate of silicon isopropoxy formation (reaction (7)). Put simply, the addition of IPA to an etchant changes the overall reaction from oxidation limited to etching limited. Unlike the very anisotropic oxidation reactions, the silicon isopropoxy etching reaction is rather isotropic, therefore the etched surface morphology is relatively rough.

The low reactivity of the silicon isopropoxy species may be due to steric hindrance by the hydrocarbon chain; however, recent unpublished results show that smaller alcohols have similar morphological effects. Of the sites in table 1, the least hindered silicon isopropoxy species, the point site, is also the most reactive. Electronic effects may play a small role in the reduced reactivity, as well. In general, the reactivity of Si—Si bonds is correlated with bond ionicity and hence with the electron-withdrawing character of the substituents (Cotton and Wilkinson 1980). For example, hydrogen-terminated silicon surfaces are stable to direct attack in acidic HF solutions, because silicon and hydrogen have very similar electronegativities (Trucks *et al.* 1990). Although the —OR functional group is somewhat less electron withdrawing than —OH (Bartmess *et al.* 1979), this difference is probably too small to account for the very different rates of $\equiv$ Si—OH and $\equiv$ Si—OR etching (reactions (4) and (10)).

Even though the IPA-enhanced etchant is relatively anisotropic, IPA selectively attacks hydrogen-terminated defect sites, such as steps and kinks. Because of this selective attack, most of the surface remains hydrogen terminated, which is consistent with the low residual carbon produced by IPA-enhanced etchants (Atluri *et al.* 1997). This defect selectivity makes direct observation of the silicon isopropoxy species very challenging. Nevertheless, motivated by the prediction of Newton *et al.* (1999), Baker *et al.* (2001) have recently observed the presence of the silicon isopropoxy species on highly miscut NH_4F/d_6-IPA-etched silicon surfaces using

Downloaded At: 16:40 21 January 2011

infrared absorption spectroscopy. This observation confirms the proposed reaction sequence.

5. Conclusions and outlook

Although the study of etchant anisotropy was stymied for decades by the lack of highly defect-sensitive surface techniques, the invention of the scanning tunnelling microscope has enabled site-specific studies of chemical reactivity. Anisotropic etching of single-crystal materials leads to a wide variety of nanoscale morphological features, such as triangular etch pits, jagged step edges and atomically flat terraces. Using a combination of STM and atomistic KMC simulations, the site-specific reaction rates that produce these features can be quantified. These reaction rates provide insights into the chemical mechanisms that govern anisotropic etching. For example, the production of atomically flat Si(111) surfaces by NH_4F etching can be explained by the existence of a pentacoordinate transition state to the initial oxidation reaction. This geometry disfavours the etching of sites held in rigid tetrahedral geometries, such as the Si(111) terrace site. Using the techniques described here, the chemistry of both simple and complex etchants can be investigated.

In spite of its profound technological importance, the development of new chemical etchants has been described as being more an art than a science. Indeed, no chemical theory of anisotropic etching exists. Although the rational control of etchant anisotropy is easily envisioned, a much more extensive database of site-specific reactivities will be needed to achieve this goal.

The nanoscale surface morphologies produced by the aqueous etchants that we have studied to date can be completely described in terms of site-specific etching reactions; however, there is good reason to believe that many etchants are more complicated. For example, many etchants produce *macroscopic* etch features, such as bunched steps and hillocks, which (apparently) cannot be explained by site-specific reactions alone. These morphologies may point to the importance of mesoscale phenomena, such as localized etchant depletion; however, much more research into this topic is needed.

Downloaded At: 16:40 21 January 2011

Acknowledgements

The work described in this article was supported by the National Science Foundation, the Beckman Young Investigator Program and the Petroleum Research Foundation. M.A.H. is a Cottrell Scholar of the Research Corporation and has been privileged to collaborate with a number of talented graduate students on this work, including Dr Jaroslav Flidr, Dr Yi-Chiau Huang, Dr Theresa A. Newton and Lori A. Lepak. Special thanks are due to the Cornell Center for Materials Research for their support and for the use of their excellent facilities, without which this research would not have been possible.

References

Allongue, P., 1996, *Phys. Rev. Lett.*, **77**, 1986.
Amelinckx, S., 1964, *The Direct Observation of Dislocations* (New York: Academic Press).
Armitage, D. A., 1982, *Comprehensive Organometallic Chemistry*, Vol. 2, edited by G. Wilkinson (Oxford: Pergamon), p. 1.

Atluri, V., Herbots, N., Dagel, D., Jacobsson, H., Johnson, M., Carpio, R., and Fowler, B., 1997, *Mater. Res. Soc. Symp. Proc.*, **477**, 281.
Baker, A. L., Chabal, Y. J., and Hines, M. A., 2001 (to be published).
Bartmess, J. E., Scott, J. A., and McIver, R. T., Jr, 1979, *J. Am. chem. Soc.*, **101**, 6046.
Batterman, B. W., 1957, *J. appl. Phys.*, **28**, 1236.
Baumhauer, H., 1894, *Die Resultate d. Ätzmethode in d. krystallographischen Forschung, an einer Reihe von krystallisierten Körpern dargestellt* (Leipzig: W. Engelmann).
Becker, R. S., Higashi, G. S., Chabal, Y. J., and Becker, A. J., 1990, *Phys. Rev. Lett.*, **65**, 1917.
Bitzer, T., Richardson, N. V., and Schiffrin, D. J., 1997, *Surf. Sci.*, **382**, L686.
Bortz, A. B., Kalos, M. H., and Lebowitz, J. L., 1975, *J. comput. Phys.*, **17**, 11.
Burkman, D. C., Deal, D., Grant, D. C., and Peterson, C. A., 1993, *Handbook of Semiconductor Wafer Cleaning Technology*, edited by W. Kern (Park Ridge, New Jersey: Noyes), p. 111.
Campbell, S. A., Cooper, K., Dixon, L., Earwaker, R., Port, S. N., and Schiffrin, D. J., 1995, *J. Micromech. Microengng*, **5**, 209.
Corriu, R. J. P., and Guerin, C., 1982, *Adv. organometal. Chem.*, **20**, 265.
Cotton, F. A., and Wilkinson, G., 1980, *Advanced Inorganic Chemistry* (New York: Wiley), chapter 12.
Dash, W. C., 1958, *Growth and Perfection of Crystals*, edited by R. H. Doremus, B. W. Roberts and D. Turnbull, (New York: Wiley) p. 361.
Elwenspoek, M., and Jansen, H. V., 1998, *Silicon Micromachining* (Cambridge University Press).
Faust, J. W., 1960, *The Surface Chemistry of Metals and Semiconductors*, edited by H. C. Gatos (New York: Wiley), p. 151.
Flidr, J., Huang, Y.-C., Newton, T. A., and Hines, M. A., 1998, *J. chem. Phys.*, **108**, 5542.
Flidr, J., Huang, Y.-C., and Hines, M. A., 1999, *J. chem. Phys.*, **111**, 6970.
Hajdasz, D. J., and Squires, R. R., 1986, *J. Am. chem. Soc.*, **108**, 3139.
Hessel, H. E., Feltz, A., Reiter, M., Memmert, U., and Behm, R. J., 1991, *Chem. Phys. Lett.*, **186**, 275.
Higashi, G. S., Chabal, Y. J., Trucks, G. W., and Raghavachari, K., 1990, *Appl. Phys. Lett.*, **56**, 656.
Higashi, G. S., and Chabal, Y. J., 1993, *Handbook of Semiconductor Wafer Cleaning Technology*, edited by W. Kern (Park Ridge, New Jersey: Noyes), p. 433.
Hines, M. A., Chabal, Y. J., Harris, T. D., and Harris, A. L., 1993, *Phys. Rev. Lett.*, **71,** 2280; 1994, *J. chem. Phys.*, **101**, 8055.
Holmes, R. R., 1990, *Chem. Rev.*, **90**, 17.
Hsiao, G. S., Virtanen, J. A., and Penner, R. M., 1993, *Appl. Phys. Lett.*, **63**, 1119.
Huang, Y.-C., 2000, PhD Dissertation, School of Applied and Engineering Physics, Cornell University, Ithaca, New York.
Huang, Y.-C., Flidr, J., Newton, T. A., and Hines, M. A., 1998a, *Phys. Rev. Lett.*, **80**, 4462; 1998b, *J. chem. Phys.*, **109**, 5025.
Jakob, P., and Chabal, Y. J., 1991, *J. chem. Phys.*, **95**, 2897.
Kaji, K., Yau, S.-L., and Itaya, K., 1995, *J. appl. Phys.*, **78**, 5727.
Kern, W., and Puotinen, D., 1970, *RCA Rev.*, **31**, 187.
Lyding, J. W., Shen, T.-C., Hubacek, J. S., Tucker, J. R., and Abeln, G. C., 1994, *Appl. Phys. Lett.*, **64**, 2010.
Merlos, A., Acero, M., Bao, M. H., Bousells, J., and Esteve, J., 1993, *Sensors Actuators* A, **37–38**, 737.
Newton, T. A., 2000, PhD Dissertation, Department of Chemistry, Cornell University, Ithaca, New York.
Newton, T. A., Huang, Y.-C., Lepak, L. A., and Hines, M. A., 1999, *J. chem. Phys.*, **111**, 9125.
Palik, E. D., Gray, H. F., and Klein, P. B., 1983, *J. electrochem. Soc.*, **130**, 956.
Pietsch, G. J., Köhler, U., and Henzler, M., 1993, *J. appl. Phys.*, **73**, 4797.
Puers, B., and Sansen, W., 1990, *Sensors Actuators* A, **21–23**, 1036.
Raghavachari, K., Jakob, P., and Chabal, Y. J., 1993, *Chem. Phys. Lett.*, **206**, 156.

Downloaded At: 16:40 21 January 2011

Rochow, E. G., 1973, *Comprehensive Inorganic Chemistry*, Vol. 1, edited by J. C. Bailar, Jr, H. J. Emeléus and R. Nyholm (Oxford, Pergamon), p. 123.
Sangwal, K., 1987, *Etching of Crystals: Theory, Experiment, and Application* (Amsterdam: Elsevier).
Schreibers, C. V., 1820, *Beitrag z. Geschichte u. Kenntnis d. meteorischen Steine u. Eisenmassen* (Wien).
Seidel, H., Csepregi, L., Heuberger, A., and Baumgärtel, H., 1990, *J. electrochem. Soc.*, **137**, 3612.
Serjeant, E. P., and Dempsey, B., 1979, *Ionisation Constants of Organic Acids in Aqueous Solution* (Oxford: Pergamon).
Shen, T.-C., Wang, C., Abeln, G. C., Tucker, J. R., Lyding, J. W., Avouris, Ph., and Walkup, R. E., 1995, *Science*, **268**, 1590.
Trucks, G. W., Raghavachari, K., Higashi, G. S., and Chabal, Y. J., 1990, *Phys. Rev. Lett.*, **65**, 504.
Tong, W. M., and Williams, R. S., 1994, *A. Rev. phys. Chem.*, **45**, 401.
Wade, C. P., and Chidsey, C. E. D., 1997, *Appl. Phys. Lett.*, **71**, 1679.
Wind, R. A., and Hines, M. A., 2000, *Surf. Sci.*, **460**, 21.

Downloaded At: 16:40 21 January 2011